

RESIDUAL STRESS IN METAL SPECIMENS PRODUCED BY DIRECT METAL LASER SINTERING

I. Yadroitsava and I. Yadroitsev

Department of Mechanical and Mechatronics Engineering, Central University of Technology,
Bloemfontein, Free State, South Africa 9300

REVIEWED

Abstract

Direct Metal Laser Sintering (DMLS) has great potential in additive manufacturing because it allows the production of full-density complex parts with the desired inner structure and surface morphology. High temperature gradients, as a result of the locally concentrated energy input, lead to residual stresses, crack formation and part deformations during processing or after separation from the supports and the substrate. In this study, an X-ray diffraction technique and numerical simulation were used for investigation of the residual stress in DMLS samples fabricated from stainless steel 316L and Ti6Al4V alloy. Conclusions regarding directions and values of stresses in DMLS objects are given.

Introduction

Direct Metal Laser Sintering (DMLS) is an additive manufacturing technology producing parts by means of a layer-by-layer method in which metal powder is pre-deposited on the building platform (substrate). The laser beam scans over the powder surface, melting the powder material and also the previous layer. Temperature gradients play a key role in the genesis of the residual stresses in DMLS objects. Many researchers have focused their attention on residual stress in DMLS parts. One of the first works in this direction was the investigation of residual stress in selective laser melting of 4140 steel by Shiomi et al. (2004). It was found that residual stresses in DMLS objects are tensile and high. Stresses can be relieved effectively by preheating of the base plate, re-scanning of each layer during manufacturing, or heat treatment in the furnace after manufacturing.

Merselis et al. (2006) studied the influence of DMLS scanning strategy on residual stress. 316L samples produced by random sector exposure (island strategy) had lower values of stresses than samples manufactured by one-scanning direction. Samples produced by one-directional strategy and separated from the substrate had stresses in perpendicular to the scanning direction significantly higher than the stresses along the scanning direction. It was found that residual stresses increased with height of samples. Residual stresses in DMLS disks produced from AISI Marage 300 steel by random sector exposure were measured using the strain gauge hole drilling method by Casavola et al. (2009). Tensile residual stresses near the surface (xy plane) were non-uniform in the specimen thickness, but for all samples the residual stress decreased sharply with the distance from the top surface. Zaeh and Branner (2010), using neutron diffractometry, studied residual stresses in cantilevers from 18Ni Maraging 300 steel as a function of the scanning strategy. The island scanning strategy caused the lowest residual stresses; a longitudinal scanning lead to the highest values of stresses. Kruth et al. (2012) suggested that the shorter scan tracks led to the smaller temperature gradient owing to the higher remnant of heat of the previous scan line.

Furumoto et al. (2010) found that DMLS of a mixture of 70% Cr-Mo steel powder, 20% Cu alloy powder and 10% Ni powder in weight results in tensile stresses within the samples and these values were extremely large at the top surface and at the boundary between the substrate and DMLS sample. Van Belle et al. (2012) proposed a numerical model to simulate the genesis of residual stresses in DMLS parts. Calculated residual stress also was higher in the top layer and in the area of the interface between the substrate.

Leuders et al. (2013) studied fatigue resistance and crack growth performance in DMLS Ti6Al4V samples. It was postulated that the main influencing factor on crack growth behaviour is residual stress. Residual stresses near the lateral surface of the samples in the building direction were nearly two times higher than the stresses in the perpendicular direction. At 100 μm -depth residual stresses were also tensile and increased significantly. Vrancken et al. (2014) investigated residual stress in DMLS Ti6Al4V compact tension specimens produced at different building strategies (xz , zx and xy direction). By using the contour method it was found that the residual stress is a major factor in the anisotropic behaviour of material produced by DMLS.

Sochalski-Kolbus et al. (2015) compared residual stress in DMLS and EBM Inconel 718 prisms. The assumption was made that some factors as a preheating, larger hatching spacing and slow cooling cause lower residual stress in EBM specimens in comparison with DMLS samples. It was indicated that crystallographic texture can have an effect on the macrostrain of AM objects and further work needs to be conducted to get a better quantitative measure of this effect.

Post-heat treatment reduced the stresses more than optimizing the parameters for the island-scanning strategy (Kruth et al., 2012). Furumoto et al. (2010) found that preheating of the substrate relieved the tensile residual stress more effectively than post heating at the top layer by the laser beam. Shot peening and surface polishing and their combination induce compressive residual stresses at the surface of DMLS samples (Sanz et al., 2008). But before stress relieving, using the heat treatment or by mechanical methods, part should be produced with a certain size, without pores, cracks and deformations. And if an algorithm for the optimal process parameters for the manufacturing of non-porous objects, using DMLS, as a whole is clear (Yadroitsev et al., 2015), the issue of the stresses during DMLS remains open. Buchbinder et al. (2014) investigated reducing distortion in DMLS by preheating during manufacturing of aluminum components. It was noted that under preheating, lower temperature gradients cause lower residual stresses, but lowered yield strength of the material at elevated temperature promotes plastic deformations. Sochalski-Kolbus et al. (2015) indicated that different process-parameters and temperature-dependent properties of the materials led to the fact that residual stress distributions at additive manufacturing are not the same from material to material and obviously process to process.

Slight deformations generally will not affect the manufacturing (Fig. 1a), but significant warp (more than the thickness of the deposited powder layer) or separation of the part from the support structures, lead to the fact that during deposition new powder layer, blade or roller will touch the deformed parts, causing even greater deformation of the parts (Fig. 2b,c). Also, the resulting vibration caused redistribution of loose powder in the form of funnels. On-line monitoring with feed-back is a vital task in the additive manufacturing technologies.

Materials and methods

Since the Centre for Rapid Prototyping and Manufacturing at Central University of Technology, Free State is specialized in producing implants, materials chosen for the study were austenitic single-phase 316L stainless steel and α/β titanium alloy Ti6Al4V, which are widely used in orthopaedic surgery, cardiovascular medicine, dentistry and general surgery.

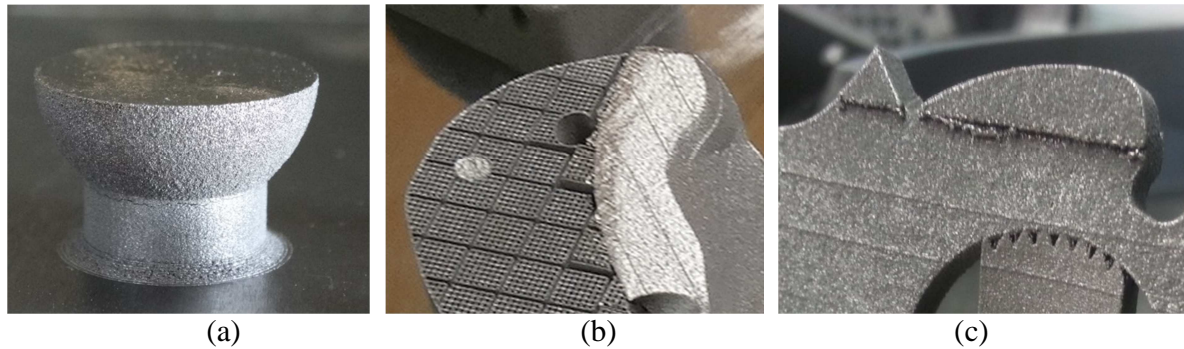


Fig. 1. Cracks (a) and deformations (b, c) of Ti6Al4V objects during DMLS.

The 316L stainless steel powder consisted of spherical particles with equivalent diameter (weight by volume) $d_{10}=3.0\ \mu\text{m}$, $d_{50}=7.1\ \mu\text{m}$ and $d_{90}=27.5\ \mu\text{m}$. The chemical composition was as follows (weight %): Fe – balance, Ni – 10-14%, Cr – 16-18%, Mo – 2-3%, Si – 0.75% max, Mn – 2% max, C – 0.03% max, P – 0.045% max, S – 0.03% max. The Ti6Al4V (ELI) powder was a pre-alloyed gas atomized powder. The chemical composition was as follows (weight %): Ti – balance, Al – 6.31%, V – 4.09%, O – 0.12%, N – 0.009%, H – 0.003%, Fe – 0.20%, C – 0.005%. The diameters (by volume) of the powder particles were $d_{10} = 13\ \mu\text{m}$, $d_{50} = 23\ \mu\text{m}$ and $d_{90} = 37\ \mu\text{m}$.

316L samples were produced at layer thickness of $40\ \mu\text{m}$ in a nitrogen atmosphere by using a one-direction scanning strategy with hatch distance of $70\ \mu\text{m}$. The Ytterbium fibre laser was 50 W, the laser spot size was $70\ \mu\text{m}$ and the scanning speed was 0.10 m/s. Ti6Al4V samples were produced by an EOSINT M280 system, also equipped with an Ytterbium fibre laser with a $80\ \mu\text{m}$ spot diameter. The laser power was 150 W, scanning speed was 1.2 m/s and the powder layer thickness was $30\ \mu\text{m}$. Back-and-forth scanning by strips with hatch distance of $100\ \mu\text{m}$ was applied for manufacturing specimens as cubes and parallelepipeds with different sizes. Argon was the protective gas for DMLS of Ti6Al4V powder. Massive substrates and powder materials were similar in chemical composition.

The residual stress measurements were done with an X-ray diffractometer from ProtoXRD. The residual stresses were determined using the $\sin^2\psi$ method. Lattice deformations of the Fe- γ {311} were determined using MnK α radiation source. The shift in the diffraction peak position at $2\theta \sim 152.3^\circ$, due to the residual stresses, was measured by the side inclination method at 5 different tilting angles ψ from -38.85 to 38.85° . Residual stresses parallel and perpendicular to the scanning direction were measured. The lattice deformations of the Ti- α were determined using a CuK α radiation source. Scans were performed around a {213} Bragg diffraction peak ($2\theta \sim 139.69^\circ$) at 9 tilting angles ψ between -44.16 + 44.16° . The residual stresses were calculated considering plan stress conditions using X-ray elastic constants (Table 1). The electrolytic removal technique was used to determine in-depth residual stress distribution. Rotation of the scanning direction is the standard strategy of the EOS, thus principal stresses and directions were analyzed.

Cross-sections of the samples were subjected to grinding with 320 SiC paper, and then polishing with diamond suspensions (9 and $3\ \mu\text{m}$ sizes), and with Silica ($0.05\ \mu\text{m}$ size). Ti6Al4V samples were etched in Kroll's reagent; for 316L samples, electro-etching in oxalic acid was used.

Table 1. Parameters used for the X-ray analysis

Test material	Collimator, mm	Wavelength, Å	Radiation	Bragg angle 2θ , °	h k l	$1/2 S_2$, MPa ⁻¹	$-S_1$, MPa ⁻¹
Fe γ	1	2.1031	Mn $K\alpha$	152.3	{311}	6.531×10^{-6}	1.429×10^{-6}
Ti α	3	1.5418	Cu $K\alpha$	139.69	{213}	11.89×10^{-6}	2.83×10^{-6}

Results and discussion

316L DMLS samples were produced using the one-direction strategy: the scanning direction (axis x) did not change during the manufacturing. All produced samples were well adhered to the substrate and low levels of porosity were observed in 5 and 25 layer samples. Figure 1 shows SEM photos of cross-sections in different planes of 25-layers samples. The solidification lines and fine microstructure are clearly visible in the horizontal cross-section of the sample (Fig. 2a). Austenite equiaxed cellular colonies with submicron-scale cells were observed in transversal cross-section of the sample (perpendicularly to the laser scanning direction, Fig. 2b). At plane zx , some colonies had an elongated shape and grew through the layers at a certain angle ($\sim 60^\circ$) regarding the laser scanning direction (Fig. 2c).

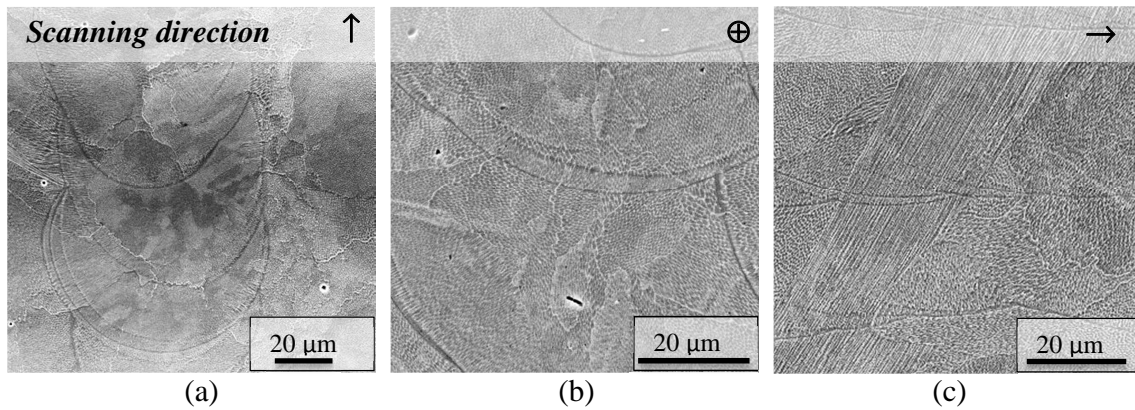


Fig. 2. Microstructure of the 316L sample at different cross-sections: xy (a), yz (b), and zx (c) planes.

When the laser beam melts powder material and the substrate, stress in the liquid molten pool is zero. The temperature of surrounding solid material near the molten pool (heat affected zone) increases. During laser melting, high compressive and tensile stresses are present under the front of the molten pool (Yadroitsev et al., 2015). Thermal conductivity defines the heat dissipation and temperature-equalization in solids. When the laser beam leaves the irradiated zone, the track begins to solidify and cool down. Various layers of material cool at different rates, therefore contraction also occurs at different speeds. Deformations in surrounding material and solidifying track occur as a result of lowered yield strength at elevated temperature of the material. Non uniform deformation of the surrounding solid material results in residual stress being present in the DMLS objects.

Surface roughness of the specimens is shown in Table 2. High roughness can have an influence on the residual stress value, so electrolytic removing of 100 μm was used to determine residual stresses in the top part of the samples. For 316L samples residual stresses were measured at the centre of the square near the surface, 100 μm in depth and near the substrate. Both stresses

along the scanning direction and in the direction perpendicular to the scanning were tensile. Shear stresses were low (± 50 MPa and lower). In samples of 5 and 25 layers the normal residual stress components acting on the x - and y -axes were $300 \div 700$ MPa and $300 \div 500$ MPa respectively at 100 μm depth (Fig. 3).

Table 2. Surface roughness of DMLS samples

	316L samples	Ti6Al4V samples
Ra	13.9 ± 3.25	4.6 ± 0.45
Rz	67.7 ± 19.96	21.9 ± 1.93

Maximal residual stresses were near the substrate, where it exceeded the value of ultimate yield strength for wrought material (500–600 MPa). Mechanical properties of DMLS part are controlled by a range of factors, but traditionally, grain refinement in the rapidly resolidified material is mainly responsible for the enhanced strength characteristics. On the whole, stresses along scanning direction were higher than in the perpendicular one. At 1–5 layers, residual stresses varied significantly in 1x1 and 3x3 cm samples. This may be due to the fact that the first few layers can differ in thickness due to roughness of the substrate and non-parallel between coater and the substrate. For 25 layers, the difference between the residual stress along scanning (σ_x) and in the perpendicular direction (σ_y) was more pronounced in 3x3 cm samples (Fig. 3).

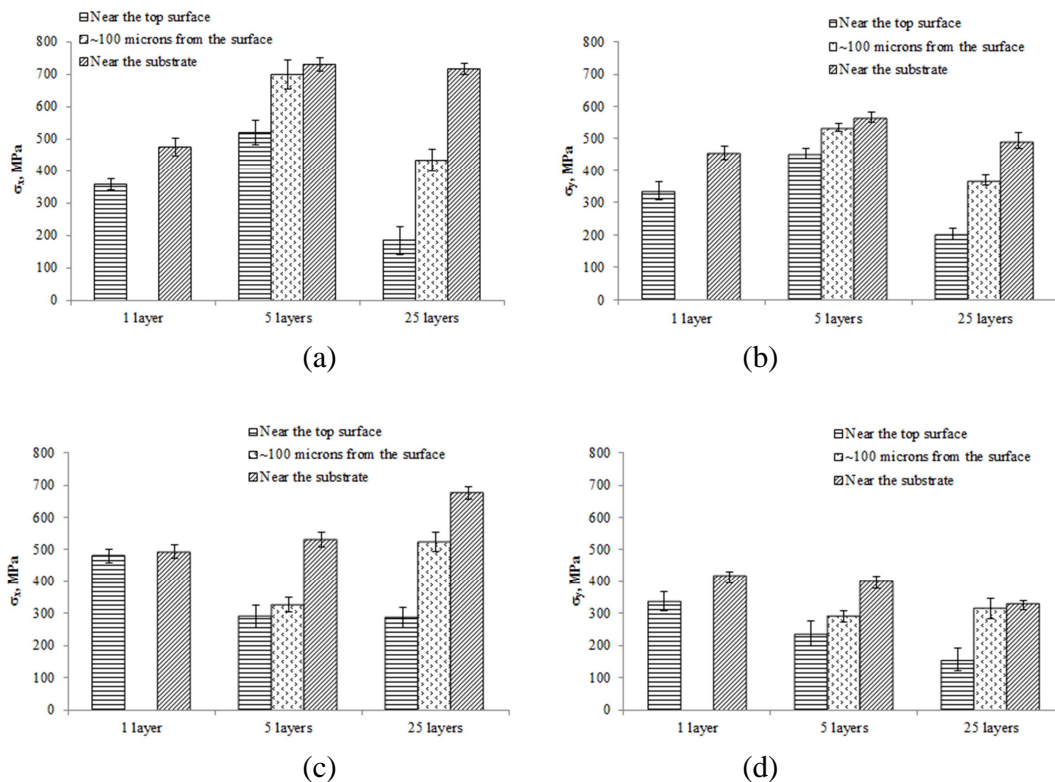


Fig. 3. Residual stresses in 316L 1x1 (a,b) cm and 3x3 cm samples (c,d).

Ti6Al4V (ELI) samples were produced at process-parameters and the strategy recommended by EOS for the M280 machine. Last layers of the parts at 90° for each layer

(“upskin” regime) were rescanned twice, without stripes. The resulting surface was smooth and surface roughness was very low (Table 2).

All produced samples had low levels of porosity. Fig. 4 shows optical microscope photos of etched cross-sections in different planes of the sample (xyz $35 \times 5 \times 20$ mm) built in z direction. A received martensitic α' microstructure is typical for Ti6Al4V samples manufactured by DMLS (Rafi et al., 2013; Simonelli et al., 2014). In the (xz) and (yz) planes a clearly visible columnar growth is observed, in the transverse direction (xy), the bundles of columnar grains are seen. The microstructure of the DMLS samples differs from the microstructure of wrought Ti6Al4V alloy since the cooling rate at DMLS reaches 10^5 – 10^6 K/s (Yadroitsava et al., 2015).

For 1×1 cm DMLS samples adhered to the substrate residual stresses near the surface measured in the central point of the surface was varied significantly with height (from 470–825 MPa for major stress and 225–420 MPa for minor stress, Fig. 5). Maximal residual stresses near the surface were practically coaxial with scanning direction.

The material strain during cooling can be described as superposition of elastic, thermal and plastic properties, as well as a creep strain component. Numerical simulations showed that, at given process parameters, the maximal temperature during the laser melting of stainless steel 316L was 2680 K and for the Ti6Al4V alloy it was approximately 3000 K (Yadroitsev et al., 2015). The heat-affected zone and the molten pool had an elongated shape in the scanning direction. The temperature gradient was more pronounced in the Ti6AlV sample than in the 316L sample due to the different thermal properties of the materials, and the energy input was higher for the Ti6Al4V alloy. Also, the residual stress near the surface in the Ti6Al4V alloy samples was higher in comparison with the 316L samples. Gusarov et al. (2013) have shown that if the deformation at the cooling stage after melting is strictly elastic, the maximum longitudinal tensile residual stresses are approximately twice as high as the maximum transverse tensile residual stresses for a narrow remelted zone. Thus, the rotation of the scanning direction in each layer allows disoriented stresses from layer to layer, but they cannot be eliminated.

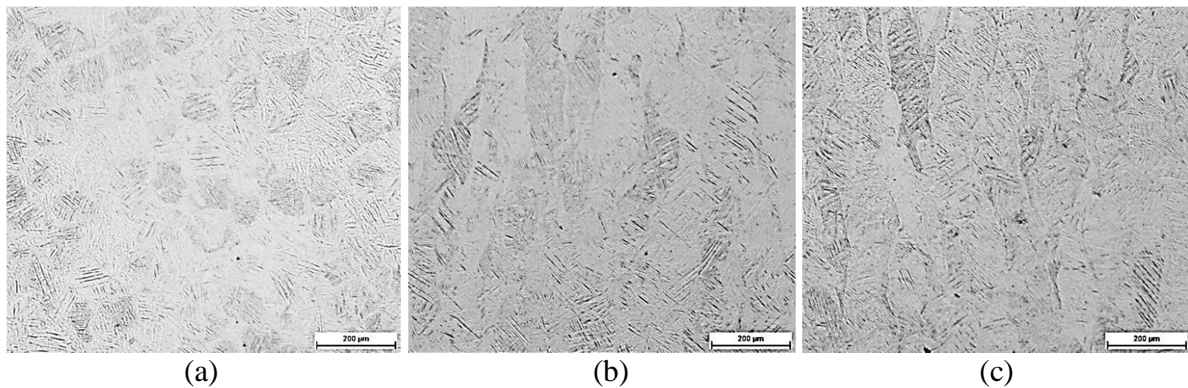


Fig. 4. Microstructure of the sample from Ti6Al4V (ELI) powder at different cross-sections: xy (a), yz (b) and xz (c) planes.

Laser scanning of the Ti6Al4V substrate led to similar residual stresses near the surface at 5 mm from the edges and in the middle point of the rectangle (Fig. 6). First principal stresses were along scanning (450–540 MPa), and second principal stresses were 130–160 MPa in perpendicular direction. In one-layer sample stresses in scanning direction for 3 points were 450–460 MPa, but stresses in perpendicular to the scanning direction varied considerably and were 70–290 MPa. The reason can be in inhomogeneity of delivered powder layer which led to

different strains during cooling. Deformations and loss of the metallurgical contact with the substrate during manufacturing led to accumulation of heat; redistribution of stresses occurred. Possibly these phenomena were the reason for a significant difference of stresses at points 1-2 and 3 in 10-layers sample.

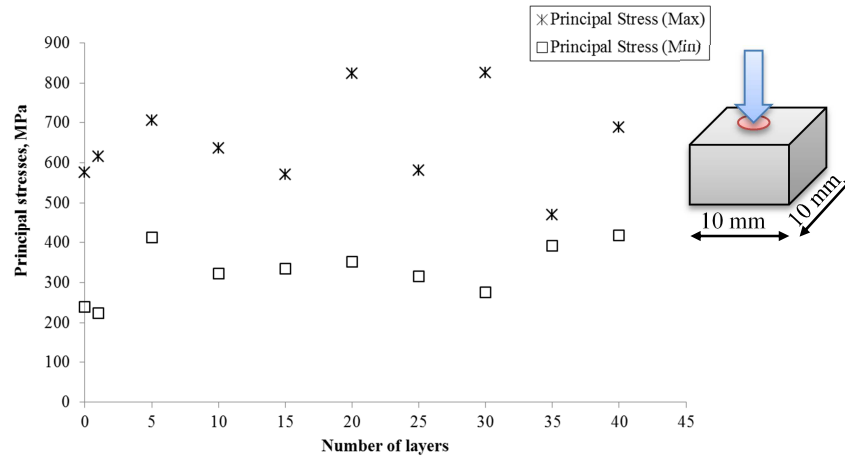


Fig. 5. Principal stresses near the surface in 1x1 cm square Ti6Al4V samples with 0–40 layers in height. Powder layer thickness was 30 μm .

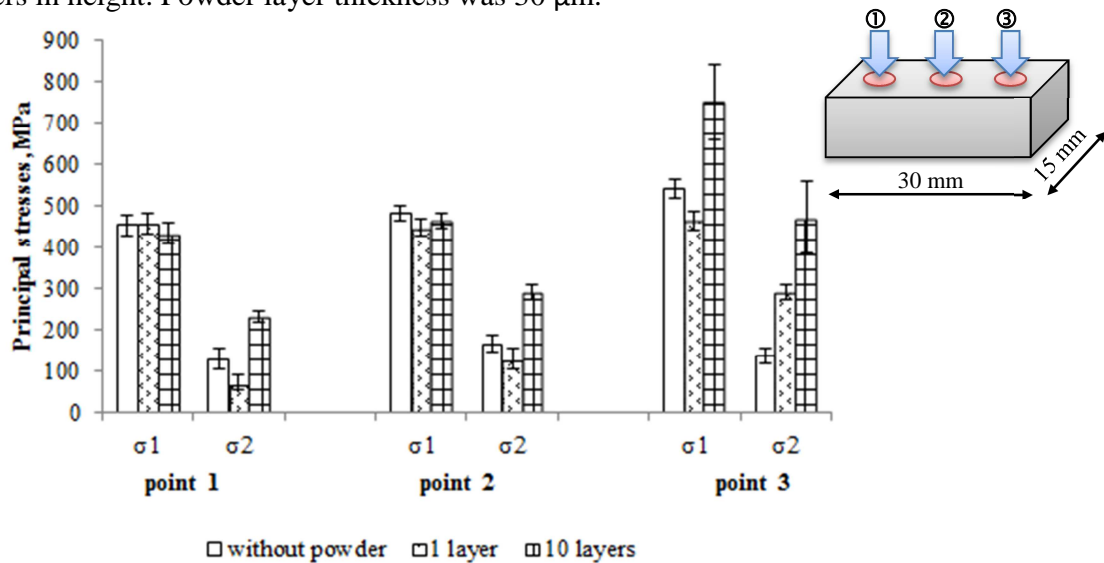


Fig. 6. Residual stresses near the surface in Ti6Al4V 1.5x3 cm rectangular samples in the different points.

Combination of high values of residual stresses of DMLS parts and imperfections such as porosity or lack of fusion between layers/supports/substrate can cause deformation and stress relaxation; it can affect the integrity of the part and its dimensions during manufacturing. Fig. 7 illustrates how imperfection 0.005 mm^3 (lack of the metallurgical contact with the substrate) can influence the stress of the part.

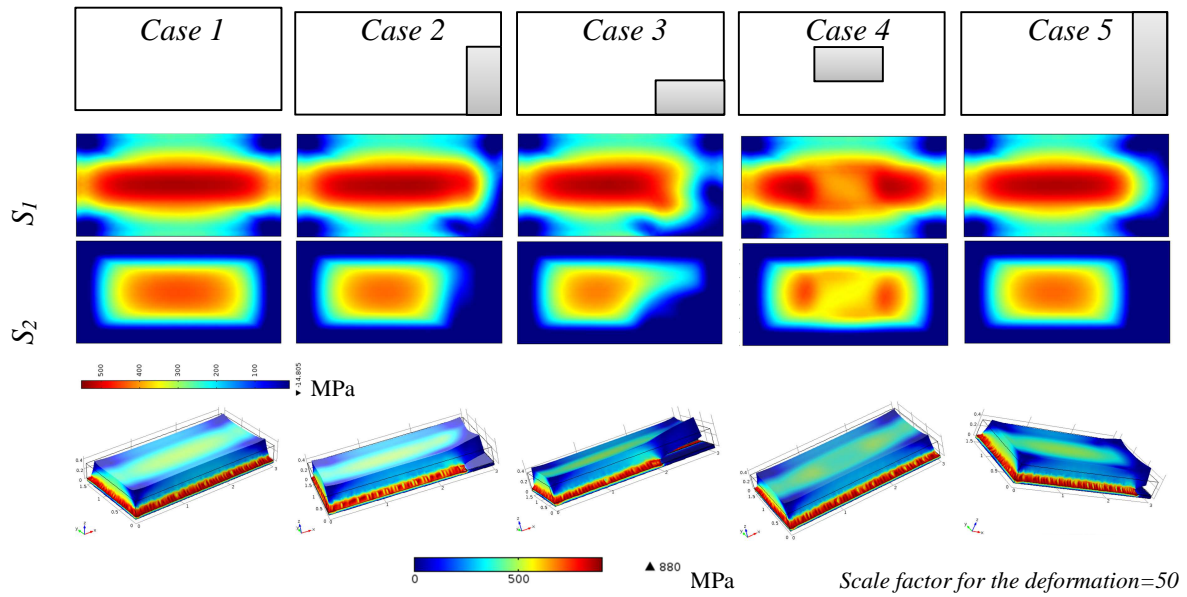


Fig. 7. Residual stresses at the top surface in the parts $3 \times 1.5 \times 0.3$ mm ($x \times y \times z$ mm) without/with imperfections. Initial stress $\sigma_{xx}=600$ MPa, $\sigma_{yy}=900$ MPa, $\sigma_{xy}=\sigma_{xz}=25$ MPa.

Relaxation of the stresses caused partial separation of the $30 \times 10 \times 10$ mm parallelepiped from the substrate (Fig. 8). Residual stresses were lower in point 3 near detaching part of the sample, which corresponds with *case 5* in Fig. 7.

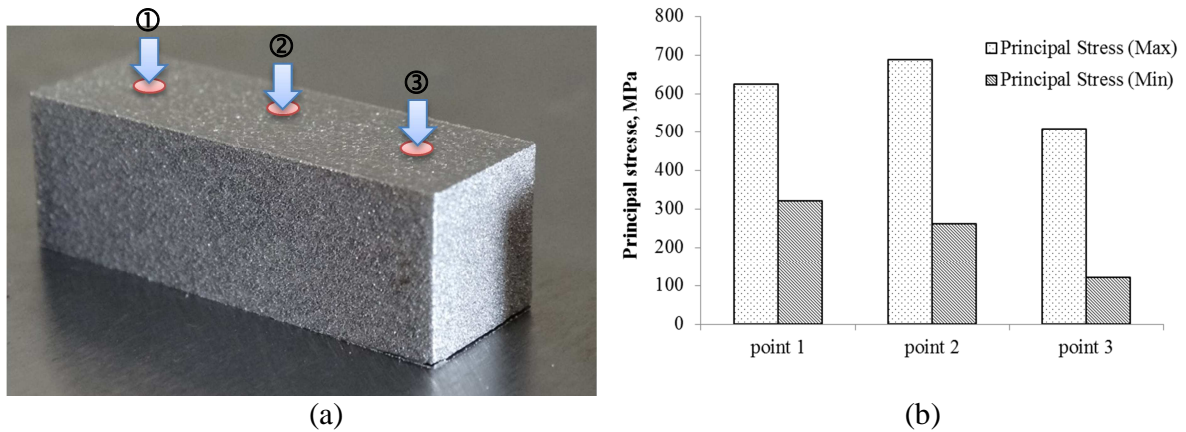


Fig. 8. DMLS Ti6Al4V (ELI) parallelepiped at the substrate (a) and principal residual stresses in 3 points near the surface.

Two cantilevers 55 mm in length, 5 mm in width and 6 mm in height were built; thin walls as a support structure had a thickness of 0.8 mm, beam had thickness of 2 mm. Additional triangular supports at the end the cantilever arms were attached, as recommended by Buchbinder et al. (2014). Residual stress near the surface were measured (Fig. 9a) in 3 points of the object: 6 mm the edges (points 1, 3) and in the middle of the top (point 2). Principal residual stresses varied greatly, maximal value was higher than residual stresses in Ti6Al4V objects manufactured

without support structures. The choice of support structures, their geometrical characteristics and positions are very important for the optimal building strategy of complex objects. Lattice structures, rigid pivots and thin walls, conical cylinders, tree-like supports lead to different thermal gradients and also the stiffness of supports and parts.

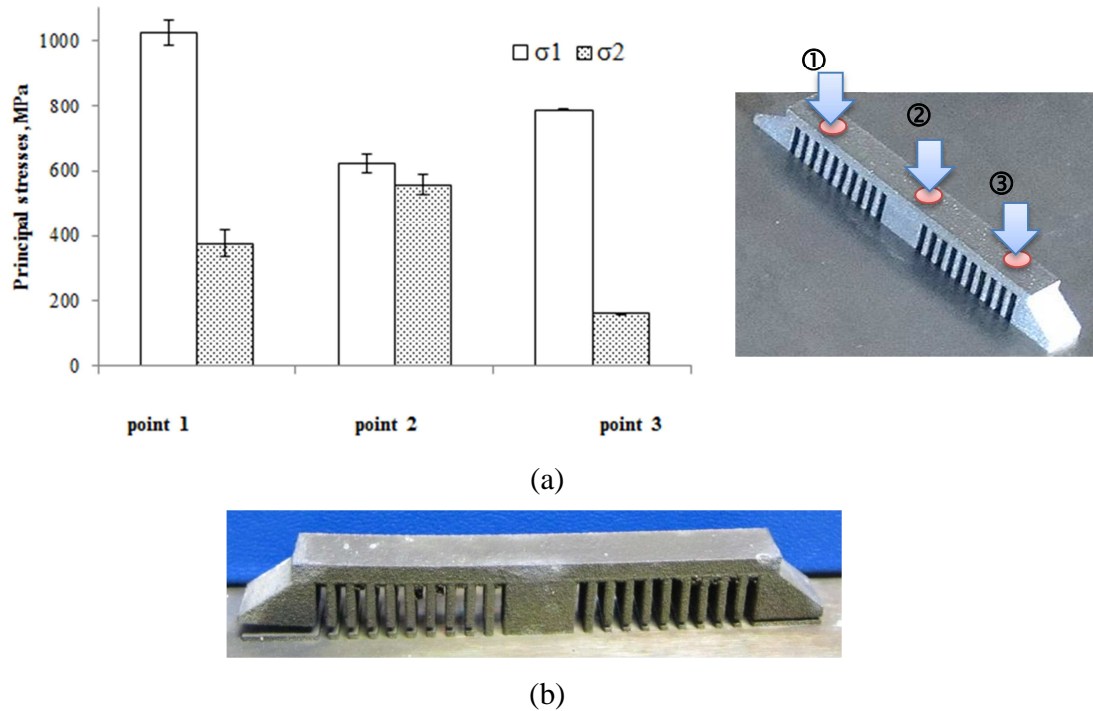


Fig. 9. XRD measured residual stresses in cantilever attached to the substrate (a) and deformation of the cantilever (b).

After cutting the right arm, the bending angle of the detached part of as-made cantilever was $0.8 \pm 0.01^\circ$. The calculated stress fields inside the deformed objects were then compared to those which caused the cantilever curl up. Yong's modulus was 113.8 GPa, Poisson's ratio was 0.342, density was 4423 kg/m^3 . Numerical simulation data agreed with that which was experimentally measured (Fig. 9). The maximal value was 970 MPa of the first principle stress; the second principal stress reached values of 429 MPa.

One of the cantilevers with the substrate was then heat treated at 650°C for 3 hours in an argon atmosphere. Then the left arm of the cantilever was detached from the substrate, it did not bend (Fig. 9b). The measured residual stresses after heat treatment in points 1-2-3 were $39 \pm 12.7 \text{ MPa}$.

Sources of uncertainty in residual stress measurements and the accuracy of calculations depends on elastic constants, non-linearity due to texture, stress gradients with depth (for example, the penetration depth for $\text{MnK}\alpha$ X-rays is near to $16 \mu\text{m}$ in austenitic stainless steel) and micro-stresses due to plastic deformation or grain interactions, etc. (Fitzpatrick et al., 2005; Fry and Lord, 2009). In the present work, experimentally measured residual stresses in DMLS specimens attached to the substrate were tensile and very high. XRD measured residual stresses had high variability.

For 316L samples, maximal residual stresses were near the substrate. Casavola et al. (2009) found that stress magnitude decreased moving towards the inner layers in DMLS disks (3-11 mm in height) produced on a base plate with supports. It was suggested that the scanning of very large number of layers may be considered as in-situ heat treatment, which relieved internal stresses. It should be noted that in the present case, specimens were thinner (2 mm max) and they were produced without supports: heat exchange with the substrate did not cause significant accumulation of heat, sufficient to relieve stress and high stiffness did not allow stress relieving by deformations.

Near the surface, principal residual stresses in Ti6Al4V samples produced at the recommended EOS process-parameters and attached to the substrate was highly variable: from 70 MPa to 1 GPa. The residual stress depends on the material properties, the geometry of the samples and the support structures, the process parameters as energy input, the powder layer thickness, the scanning strategy, preheating, etc. The direction of major stress also was coaxed with the scanning direction. This should be taken into account when choosing strategy for sintering objects with complex shapes, positioning them on the substrate and the definition support structures of the DMLS parts.

Conclusions

Residual stresses in as-built DMLS 316L and Ti6Al4V, measured by the XRD method in *xy* plane, were biaxial tensile stresses. Samples had residual stresses even higher than the value of ultimate yield strength for wrought materials. The major component was coaxial with scanning direction.

Before separation from the substrate, all DMLS samples, especially those with fine structured parts, must be heat treated to avoid significant deformation. During manufacturing, heat treatment is seen as the main way to reduce residual stresses in DMLS parts. Determination of optimal conditions for different materials to reduce the residual stresses during manufacturing and to obtain acceptable performance properties of DMLS parts are the subject for further in-depth studies in DMLS.

Acknowledgements

This work is based on the research supported by the South African Research Chairs Initiative of the Department of Science and Technology and National Research Foundation of South Africa (Grant №97994) and the Collaborative Program in Additive Manufacturing (Contract №CSIR-NLC-CPAM-15-MOA-CUT-01).

References

- [1] Buchbinder, D. Meiners, W. Pirch, N., Wissenbach, K. and Schrage J. (2014). Investigation on reducing distortion by preheating during manufacture of aluminum components using selective laser melting, *Journal of Laser Applications* 26:012004.
- [2] Casavola C, Campanelli S L and Pappalettere C. (2009). Preliminary investigation on distribution of residual stress generated by the selective laser melting process. *The Journal of Strain Analysis for Engineering Design* 2009 44: 93.

- [3] Fitzpatrick M. E., Fry, A. T., Holdway, P., Kandil, F. A., Shackleton, J., Suominen, L. (2005). Determination of residual stresses by X-ray diffraction. A National Measurement Good Practice Guide, 52(2), 68 p.
- [4] Fry, A. T., Lord, J. D. (2009). Measuring residual stresses in stainless steel—recent experiences within a VAMAS exercise. *Powder Diffraction*, 24: S41-S44. doi:10.1154/1.3133146.
- [5] Furumoto, T., Ueda, T., Abdul Aziz M.S., Hosokawa, A., Tanaka, R., (2010). Study on reduction of residual stress induced during rapid tooling process: influence of heating conditions on residual stress. *Key Engineering Materials*, V. 447-448: 785-789.
- [6] Gusarov, A., Malakhova-Ziablova, I., Pavlov, M. (2013). Thermoelastic residual stresses and deformations at laser treatment. *Physics Procedia*, 41: 889–896.
- [7] Kruth, J.-P., Deckers, J., Yasa, E. and Wauthle, R. (2012). Assessing and comparing influencing factors of residual stresses in selective laser melting using a novel analysis method, *Proc IMechE Part B: J Engineering Manufacture*, 0(0) 1–12, Catholic University of Leuven 2012, doi: 10.1177/0954405412437085.
- [8] Leuders S., Thöne, M. Riemer A., Niendorf T., Tröster T., Richard H.A., Maier H.J. (2013). On the mechanical behaviour of titanium alloy TiAl6V4 manufactured by selective laser melting: Fatigue resistance and crack growth performance. *International Journal of Fatigue*. 48: 300–307.
- [9] Mercelis, P. and Kruth, J.-P. (2006). Residual stresses in selective laser sintering and selective laser melting. *Rapid Prototyping Journal*, 12 (5): 254 – 265.
- [10] Rafi H.K., Karthik N.V., Gong, H., Starr, T. L. and Stucker, B. E. (2013). Microstructures and Mechanical Properties of Ti6Al4V Parts Fabricated by Selective Laser Melting and Electron Beam Melting. *Journal of Materials Engineering and Performance* 22(12): 3873-3883.
- [11] Sanz, C. and García Navas, V. (2013). Structural integrity of direct metal laser sintered parts subjected to thermal and finishing treatments. *Journal of Materials Processing Technology*, 213(12): 2126–2136.
- [12] Shiomi, M., Osakada, K., Nakamura, K., Yamashita, T. & Abe, F. (2004). Residual stress within metallic model made by Selective Laser Melting process. *CIRP annals - Manufacturing technology* 53(1):195-198.
- [13] Simonelli, M., Tse, Y.Y., Tuck, C. (2014). Effect of the build orientation on the mechanical properties and fracture modes of SLM Ti–6Al–4V. *Materials Science & Engineering A* 616 1–11.
- [14] Sochalski-Kolbus, L.M., Payzant, E.A., Cornwell, P.A., Watkins, T.R., Babu, S.S., Dehoff, R.R., Lorenz, M., Ovchinnikova, O., Duty, C. (2015). Comparison of residual stresses in Inconel 718 simple parts made by Electron Beam Melting and Direct Laser Metal Sintering. *Metallurgical and materials transactions A*. 46(3): 1419-1432.
- [15] Van Belle, L., Vansteenkiste, G. Boyer, J.-C., 2012. Comparisons of numerical modelling of the Selective Laser Melting. *Key Engineering Materials*, 504-506: 1067.
- [16] Vrancken, B., Cain, V., Knutsen, R., Van Humbeeck, J. (2014). Residual stress via the contour method in compact tension specimens produced via selective laser melting. *Scripta Materialia*, 87: 29–32.
- [17] Yadroitsava, I., Grewar, S., Hattingh, D., Yadroitsev, I. (2015). Residual stress in SLM Ti6Al4V alloy specimens. *Materials Science Forum*, 828-829: 305-310.

- [18] Yadroitsev, I., Yadroitsava, I. (2015). Evaluation of residual stress in stainless steel 316L and Ti6Al4V samples produced by selective laser melting, *Virtual and Physical Prototyping*, DOI: 10.1080/17452759.2015.1026045.
- [19] Yadroitsev, I., Krakhmalev, P., Yadroitsava, I. (2014). Hierarchical design principles of selective laser melting for high quality metallic objects. *Additive Manufacturing*. doi:10.1016/j.addma.2014.12.007.
- [20] Zaeh, M. F., Branner, G. (2010). Investigations on residual stresses and deformations in selective laser melting. *Production Engineering - Research and Development*, 4: 35–45.